Co@N-CNT/MXene in situ grown on carbon nanotube film for multifunctional sensors and flexible supercapacitor

Qiufan Wang[#], Jiaheng Liu[#], Guofu Tian, Daohong Zhang[*]

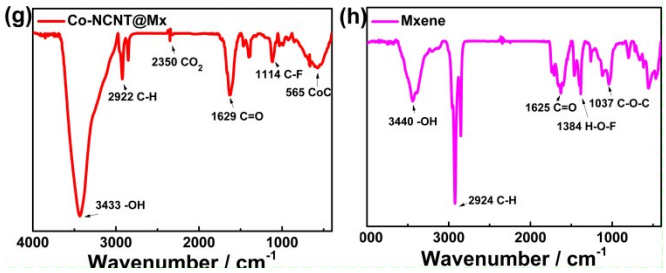

Fig. S1. FTIR spectrum of $Ti_3C_2T_x$ MXene nanosheets and Co@N-CNT/MXene.

Fig.S1a-b are FT-IR datas. Comparing the composite material and $Ti_3C_2T_x$ MXene, it can be clearly seen that the composite material has a residual C-F absorption peak at 1114 cm^{-1}, and a new Co-C absorption peak at 565 cm^{-1}, which is located at 1384 cm^{-1} and 1037 cm^{-1}, respectively. The H-O-F and C-O-C disappeared. Based on the above analysis, it can be confirmed that the process of composite synthesis is successed.

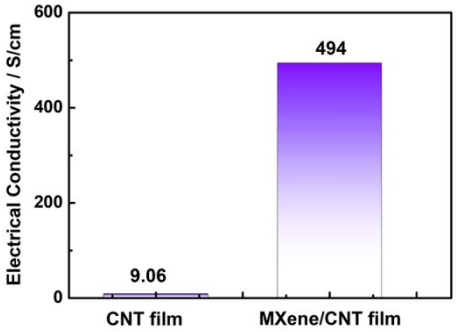

Fig. S2 Conductivity of CNT film and MXene/CNT film.

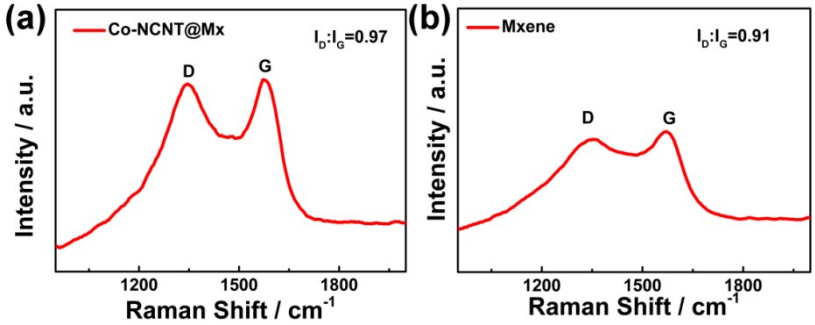

Fig. S3 The Raman spectrum of Co-NCNT@Mx and $Ti_3C_2T_x$ MXene at the laser wavelength is 633 nm.

Co@N-CNT/MXene has two prominent peaks at ≈1350 cm^{-1} (D peak) and ≈1597 cm^{-1} (G peak). The observed D peak corresponds to the breathing pattern of carbon in carbon nanotubes and is attributed to Defects and local disorder after nitrogen doping. The ratio of the intensity of the D peak to the G peak (I_D/I_G) is 0.97. In the Raman spectrum of $Ti_3C_2T_x$ MXene, the D peak at 1347 cm^{-1} can be attributed to the in-plane change of the C-Ti bond, while the G peak shifts to around 1578cm^{-1}, and I_D/I_G decreases to 0.91, it shows that the chemical structure changes brought about by the composite material lead to the increase of disorder and defects.

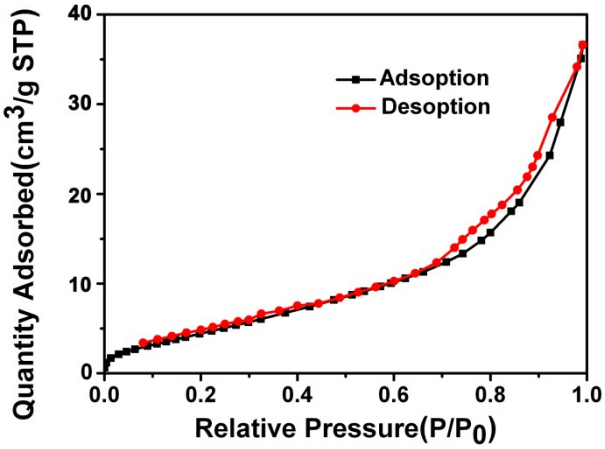

Fig. S4 N_2 adoption and desorption isotherm curve of the Co@N-CNT/MXene electrode.

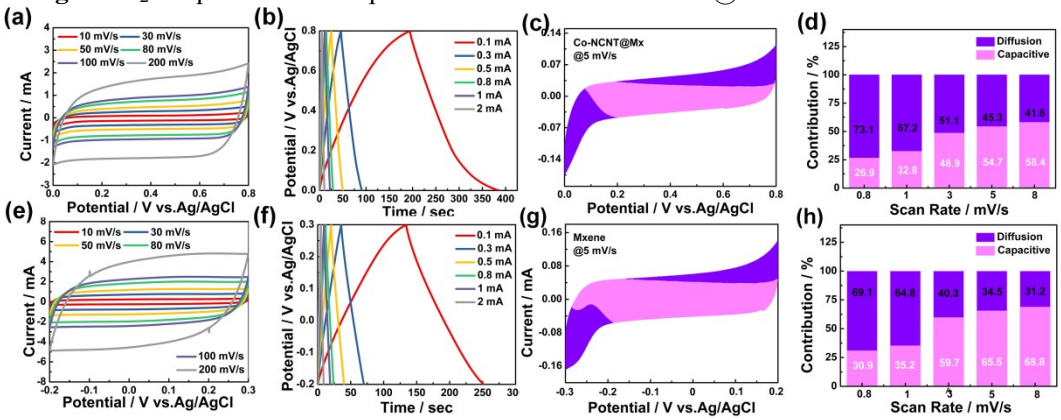

Fig. S5 Electrochemical properties of electodes. (a, e) CV curves of Co@N-CNT/MXene and $Ti_3C_2T_x$ MXene; (b, f) GCD of the Co@N-CNT/MXene and $Ti_3C_2T_x$ MXene; (c, g) surface-limited and diffusion-limited charge storage contributions for Co@N-CNT/MXene and $Ti_3C_2T_x$ MXene at 5 mV s^{-1}; (d, h) Capacity ratios of diffusion-controlled and surface capacitive charge for Co@N-CNT/MXene and $Ti_3C_2T_x$ MXene at 0.8 to 8 mV s^{-1}.

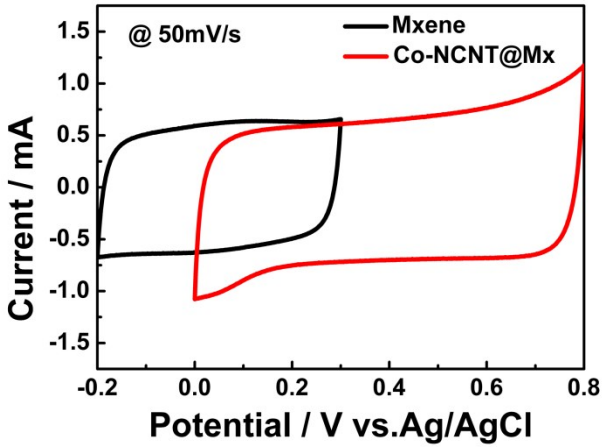

Fig. S6 The CV curves of Co@N-CNT/MXene and $Ti_3C_2T_x$ MXeneat 50 mV s^{-1}.

Fig. S5a-b show the cyclic voltammetry (CV) and constant current charge and discharge (GCD) tests of Co@N-CNT/MXene. Comparing Fig. S5e-f, it can be seen that the voltage window of the composite material increases from -0.3 to 0.2 V to 0 to 0.8 V. The charge-discharge time is increased from 250 s to 375 s. As shown in Fig. S6, which is the comparison of CV curves between Co@N-CNT/MXene and $Ti_3C_2T_x$ MXene electrode materials at 50 mV s^{-1}. The CV curve area of Co@N-CNT/MXene is twice larger than $Ti_3C_2T_x$ MXene. In order to study the electrochemical kinetics of Co@N-CNT/MXene and $Ti_3C_2T_x$ MXene electrodes, the CV was used to measure different scan rates from 0.8 to 8 mV s^{-1}. This means that the electrical properties of Co@N-CNT/MXene and

$Ti_3C_2T_x$ MXene are derived from the diffusion control process and capacitive behavior. As shown in Fig. S5c&g, it can be observed that the ion diffusion ratio of Co@N-CNT/MXene is higher than that of $Ti_3C_2T_x$ MXene at a scan rate of 5 mV s^{-1}, indicating the excellent ion transmission rate of the composite material. And the cycle stability is better than $Ti_3C_2T_x$ MXene at high scanning rate. In fact, the scan rate and peak current obey the following relationship: $i=av^b$, which can be rewritten as: $log(i)=blog(v)+log(a)$. Among them, i (mA) represents the peak current, v (mV s^{-1}) represents the scan rate, and a and b are adjustable parameters. The relationship between b value and $log(i)$ and $log(v)$ related to different redox peaks can be calculated linearly. In order to further analyze the electrochemical kinetics of Co@N-CNT/MXene and $Ti_3C_2T_x$ MXene, we also use the following formula to perform diffusion control and quantitative analysis of capacitive contribution to the current response: $i=k_1v+k_2v^{1/2}$, among them, k_1v is attributed to the surface capacitance process, and $k_2v^{1/2}$ corresponds to the diffusion control intercalation. In Fig. S5d&h, it can be seen that the ion diffusion rate of Co@N-CNT/MXene is greater than that of $Ti_3C_2T_x$ MXene at all scanning rates. As the scann rate gradually increased, the surface capacitance ratio of Co@N-CNT/MXene gradually increased from 26.9% to 58.4%, which were all smaller than the surface capacitance ratio of pure $Ti_3C_2T_x$ MXene, reflecting the rapid reaction kinetics of Co@N-CNT/MXene.

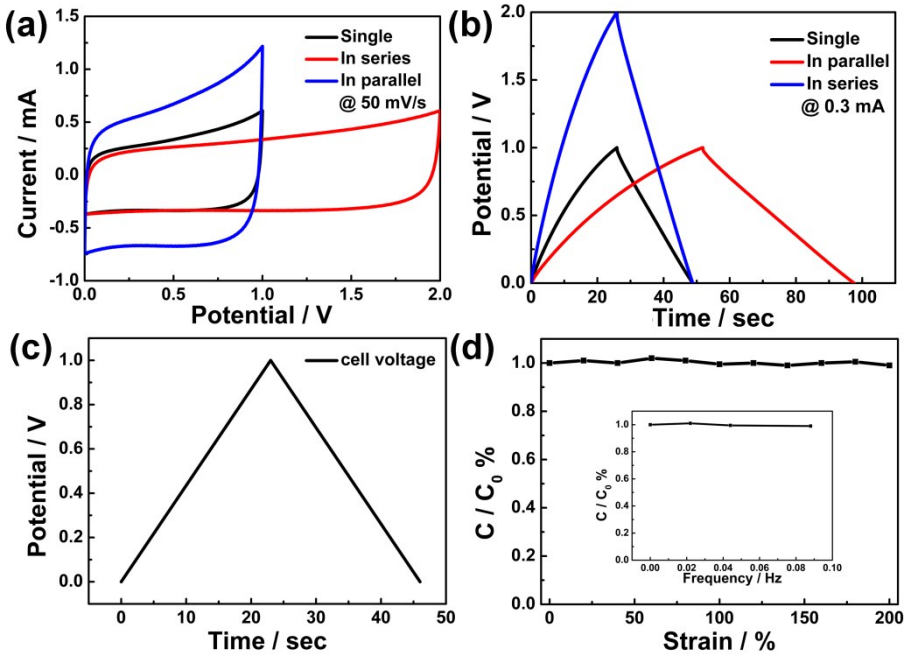

Fig. S7 Electrochemical characteristics of the Co-NCNT@Mx symmetry SC: (a,b) CV and GCD curves of individual and connected devices; (c) The changes of the strain distance and GCD versus time in Fig S7 (d) SC capacitance retention rate under different stretching rate and stretching frequency.

After discussing the performance of the composite electrode material, we combined Co@N-CNT/MXene electrode material and LiCl/PVA gel electrolyte to form a stretchable flexible symmetrical SC, and conducted a series of electrochemical and mechanical properties. The CV and CD curves of Fig. S7a-b show that two devices in series can provide twice the voltage window of a single device, or devices in parallel can provide twice the discharge time of a single device at the same current density It is twice the maximum power of a single device. The SC was determined by up to 200% strain and different stretching frequencies (Fig. S7c). In addition, the SC was tested for capacitance retention under different stretching rates (Fig. S7d). Among them, under different stretching frequencies at 200% stretching rate, the capacitance retention rate of the device does not change significantly, and C/C_0 is basically maintained at about 1. Under different stretch rates, the capacitance retention rate of the device fluctuates around 1.

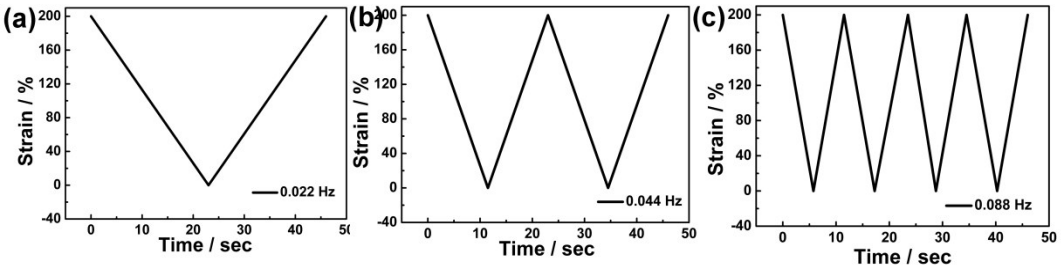

Fig. S8 The changes of the strain distance and cell voltage *vs.* time.

Figure S8 shows the relationship between strain and SC voltage with respect to time at different dynamic frequencies. At the beginning (0 s), the strain and voltage of the device were 200% and 0 V, respectively. The strain then decreases, and the device voltage increases linearly with time. At 23 s, the device voltage is 1 V (f = 0.022 Hz), completing a bending cycle. At 46 s, after another bending cycle, the strain increased to 200% and the voltage returned to 0 V.